Tuning the glass-forming ability of metallic glasses through energetic frustration

Yuan-Chao Hu,[1] Jan Schroers,[1] Mark D. Shattuck,[2] and Corey S. O'Hern[1,3,4,*]

[1]*Department of Mechanical Engineering & Materials Science, Yale University, New Haven, Connecticut 06520, USA*

[2]*Benjamin Levich Institute and Physics Department, The City College of New York, New York, New York 10031, USA*

[3]*Department of Physics, Yale University, New Haven, Connecticut 06520, USA*

[4]*Department of Applied Physics, Yale University, New Haven, Connecticut 06520, USA*

(Received 7 April 2019; revised manuscript received 24 July 2019; published 14 August 2019)

The design of multifunctional bulk metallic glasses is limited by the lack of a quantitative understanding of the variables that control the glass-forming ability of alloys. Both geometric frustration (e.g., differences in atomic radii) and energetic frustration (e.g., differences in the cohesive energies of the atomic species) contribute to the glass-forming ability. We perform molecular dynamics simulations of binary Lennard-Jones mixtures with only energetic frustration. We show that there is little correlation between the heat of mixing $\Delta H_{\rm mix}$ and critical cooling rate R_c, below which the system crystallizes, except that $\Delta H_{\rm mix} < 0$. By removing the effects of geometric frustration, we show strong correlations between R_c and the variables $\epsilon_- = (\epsilon_{BB} - \epsilon_{AA})/(\epsilon_{AA} + \epsilon_{BB})$ and $\overline{\epsilon}_{AB} = 2\epsilon_{AB}/(\epsilon_{AA} + \epsilon_{BB})$, where ϵ_{AA} and ϵ_{BB} are the cohesive energies of atoms A and B and ϵ_{AB} is the pair interaction between A and B atoms. We identify a particular composition-dependent combination of ϵ_- and $\overline{\epsilon}_{AB}$ that collapses the data for R_c over nearly 4 orders of magnitude in cooling rate. By performing local structural analyses, we find that energetic frustration, even in the absence of geometric frustration, can induce short-range fivefold symmetric order that impedes crystallization. This result emphasizes that energetic frustration plays an important role in determining the glass-forming ability, and thus it should be taken into account in the design of new metallic glass formers.

DOI: 10.1103/PhysRevMaterials.3.085602

I. INTRODUCTION

Bulk metallic glasses (BMGs) are amorphous alloys that possess promising structural, mechanical, and functional properties [1–3]. However, a given BMG may not possess multiple desirable properties, such as high elastic strength and biocompatibility in the case of BMGs used in biomedical applications [4]. Thus, *de novo* design of BMGs with multifunctional properties is an important goal. A key impediment to progress is that one cannot currently predict the glass-forming ability (GFA) of a given alloy [5]. The GFA can be directly quantified by measuring the critical cooling rate R_c, below which the system crystallizes. Smaller R_c implies better GFA. The most prominent and widely used features for identifying BMGs were suggested by Inoue in 2000 [6]: (1) BMGs are typically multicomponent systems consisting of three or more elements, (2) the size ratios of the three main constituents differ by more than 12%, and (3) the heat of mixing $\Delta H_{\rm mix}$ among the three main elements is negative. However, there are many examples of metallic glasses that do not obey these rules. First, several binary alloys (such as CuZr) possess GFAs that are comparable to those for multicomponent BMGs [7–9]. Also, there are many ternary alloys (e.g., Al, Cu, and V) that have $R_c < 10^6$ K/s, but the diameter ratios among the three elements differ by less than 12% [10]. Furthermore, recent experimental studies have shown that even monoatomic metallic systems can form glasses via rapid cooling [11]. Thus, it is clear that a more quantitative theoretical framework is necessary for predicting the GFA of alloys.

There are two main contributions to the GFA of an alloy, geometric and energetic frustration [12,13]. Geometric frustration can be achieved in alloys using elements with sufficiently different metallic radii [12,14,15], which allows the glass phase to pack more densely, but severely strains the competing crystalline phases. Energetic frustration can be achieved in alloys even with elements of similar sizes, if they possess different cohesive energies and strong interactions between different atomic species. While there have been many computational studies of the variation of R_c with geometric frustration [13,16,17], there are few studies that have investigated how energetic frustration in the absence of geometric frustration affects the GFA.

In this study we carry out molecular dynamics simulations of binary Lennard-Jones (LJ) mixtures with atoms of the same size, but different cohesive energies, to understand the critical cooling rate as a function of the degree of energetic frustration. We find several important results: (1) We show that there is little correlation between the GFA and heat of mixing in binary and multicomponent metallic glass formers. (2) Instead, we find that there is a particular combination of the difference in the cohesive energies and the pair interactions among different species in binary alloys that yields the best GFA for each composition. (3) We rationalize these findings for binary LJ systems with the best GFA by considering separation fluctuations and chemical ordering [18] among nearest neighbor atoms. We also show that energetic frustration, even in the absence of geometric frustration, gives

*corey.ohern@yale.edu

rise to local fivefold symmetric structural order that impedes crystallization.

II. METHODS

We focus on binary LJ mixtures in three dimensions with vanishing geometric, but tunable energetic frustration. The pairwise interaction potential is

$$V(r_{ij}) = 4\epsilon_{ij}\left[\left(\frac{\sigma}{r_{ij}}\right)^{12} - \left(\frac{\sigma}{r_{ij}}\right)^{6}\right], \tag{1}$$

where σ is the diameter of atoms A and B, r_{ij} is the separation between atoms i and j, ϵ_{AA} and ϵ_{BB} are the cohesive energies of atoms A and B, and ϵ_{AB} is the interaction energy between A and B. The potential is truncated and shifted at $r_{ij} = 2.5\sigma$, and the total potential energy is $V = \sum_{i>j} V(r_{ij})$. We consider $N = N_A + N_B$ atoms with equal mass $m_A = m_B$ in a cubic box and periodic boundary conditions in all directions. We carry out simulations with $N = 1000$, 2000, and 4000 to investigate system-size effects; we show in the Appendix that the system-size dependence of the critical cooling rate R_c is weak. Length, energy, pressure, and time scales will be reported in units of σ, ϵ_{AA}, ϵ/σ_{AA}^3, and $\sqrt{m_A\sigma^2/\epsilon_{AA}}$.

We first equilibrate each system with fraction of B atoms, $f_B = N_B/N$, and combinations of $\epsilon_{BB}/\epsilon_{AA}$ and $\epsilon_{AB}/\epsilon_{AA}$ at high temperature $T = 5.0$ (using a Nose-Hoover thermostat [19,20]) and then quench them to low temperature $T = 0.01$ as a function of cooling rate R. The thermal quenches are performed at fixed pressure $P_0 = 10$ to avoid cavitation [21], and the results are averaged over six independent simulations. As shown in the Appendix, we find that the particular value of P_0 does not strongly affect the GFA in systems that do not cavitate over the range $10^{-2} < P_0 < 10$.

III. RESULTS AND DISCUSSION

To understand the relevant range of parameter space for the cohesive energies ϵ_{AA} and ϵ_{BB}, and interaction energy ϵ_{AB}, we cataloged these values for 990 binary alloys involving 45 elements that occur in metallic glasses. For this analysis, we chose element A such that $\epsilon_{AA} > \epsilon_{BB}$ and used the pairwise definition of the heat of mixing $\Delta H_p(i,j) = (\epsilon_{ii} + \epsilon_{jj})/2 - \epsilon_{ij}$ to calculate ϵ_{AB} [22]. Values for ϵ_{AA}, ϵ_{BB}, and ΔH_p were obtained from experimental data [23,24]. In Fig. 1(a) we show that binary alloys exist over a relatively narrow range of parameters $0.5 \lesssim \epsilon_{AB}/\epsilon_{AA} \lesssim 1.4$ and $0.1 \lesssim \epsilon_{BB}/\epsilon_{AA} < 1$. In contrast, these energetic parameters can exist over a wider range in ionic liquids and molten salts [25,26]. Albeit with scatter, the experimental data scales as $\epsilon_{AB} \propto \sqrt{\epsilon_{AA}\epsilon_{BB}}$, which is similar to the London mixing rule $\epsilon_{AB} = \chi_{\rm London}\sqrt{\epsilon_{AA}\epsilon_{BB}}$ [27], where

$$\chi_{\rm London} = \frac{2\sqrt{I_A I_B}}{I_A + I_B}\left[\frac{2\sqrt{\sigma_{AA}\sigma_{BB}}}{\sigma_{AA} + \sigma_{BB}}\right]^6, \tag{2}$$

$\sigma_{ij} = (\sigma_i + \sigma_j)/2$ is the average diameter of atoms i and j, and I_A and I_B are the ionization energies of atoms A and B. In Fig. 1(b) we show the ratio of $\chi_{\rm expt} = \epsilon_{AB}/\sqrt{\epsilon_{AA}\epsilon_{BB}}$ for the experimental data to $\chi_{\rm London}$. More than 70% of the data obeys the London mixing rule with $1 < \chi_{\rm expt}/\chi_{\rm London} < 1.25$.

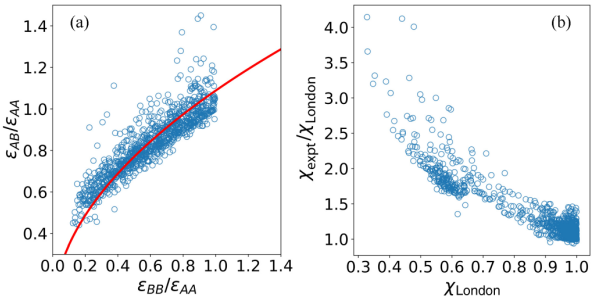

FIG. 1. (a) The interaction energy ϵ_{AB} (normalized by ϵ_{AA}) from the pairwise heat of mixing ΔH_p plotted versus the cohesive energy ratio $\epsilon_{BB}/\epsilon_{AA}$ for 990 binary alloys involving 45 elements found in metallic glasses [23,24]. We chose element A, such that $\epsilon_{AA} > \epsilon_{BB}$. The solid line obeys $\epsilon_{AB} = c\sqrt{\epsilon_{BB}\epsilon_{AA}}$ with $c = 1.09$. (b) The ratio of $\chi_{\rm expt} = \epsilon_{AB}/\sqrt{\epsilon_{AA}\epsilon_{BB}}$ to the London expression $\chi_{\rm London}$ in Eq. (2), plotted versus $\chi_{\rm London}$ for the same data in (a).

To more fully understand the effects of energetic frustration on the GFA of binary mixtures, below we independently vary $\epsilon_{AB}/\epsilon_{AA}$ and $\epsilon_{BB}/\epsilon_{AA}$ over a much wider range than in Fig. 1(a).

To quantify the GFA, we analyze the positional order of the system by measuring the bond orientational order parameter for atom i [28,29]:

$$Q_6(i) = \left[\frac{4\pi}{13}\sum_{m=-6}^{m=6}\left|\frac{1}{N_i+1}\left(q_{6m}(i) + \sum_{j=1}^{N_i} q_{6m}(j)\right)\right|^2\right]^{1/2}, \tag{3}$$

where $q_{6m}(i) = N_i^{-1}\sum_{j=1}^{N_i}(A_j^i/A_{\rm tot}^i)Y_{6m}[\theta(\boldsymbol{r}_{ij}), \phi(\boldsymbol{r}_{ij})]$, $Y_{6m}[\theta(\boldsymbol{r}_{ij}), \phi(\boldsymbol{r}_{ij})]$ is the spherical harmonic of degree 6 and order m, θ is the polar angle and ϕ is the azimuthal angle of the vector $\boldsymbol{r}_{ij}$ from atom i to j, N_i is the number of Voronoi neighbors of atom i, A_j^i is the area of the Voronoi cell face separating atoms i and j, and $A_{\rm tot}^i$ is the total area of all faces of the Voronoi cell for atom i [29].

The bond orientational order can distinguish between disordered systems ($Q_6 \lesssim 0.3$) and systems with crystalline order [e.g., face-centered cubic (fcc) with $Q_6 = 0.575$, body-centered cubic (bcc) with $Q_6 = 0.511$, and hexagonal close packed (hcp) $Q_6 = 0.485$]. In Fig. 2(a) we show the fraction f of each sample with local fcc, hcp, bcc, and disordered structure (using adaptive common neighbor analysis [30]) in systems with $f_B = 0.5$ over the full range of cohesive and interaction energies for $R = 5\times10^{-5}$. For more than 80% of the systems, the fraction of atoms with fcc or hcp order exceeds 0.70, whereas very few atoms possess bcc order. (We verify this result for other cooling rates in the Appendix.) In Fig. 2(b) we plot the distribution $P[Q_6(i)]$ for a system with $\epsilon_{BB}/\epsilon_{AA} = \epsilon_{AB}/\epsilon_{AA} = 1$ and several R. For $R > R_c$, the systems are disordered and $P[Q_6(i)]$ has a peak near $Q_6 \approx 0.2$. For $R < R_c$, $P[Q_6(i)]$ develops peaks near the values corresponding to fcc and hcp order. The peak near $Q_6(i) \approx 0.535$ corresponds to regions of adjacent fcc and hcp order, not to bcc order as shown in the Appendix. In Fig. 2(c) we show that $\langle Q_6\rangle = N^{-1}\sum_{i=1}^{N} Q_6(i)$ versus R is similar to a logistic function, and R_c corresponds to the cooling rate at which

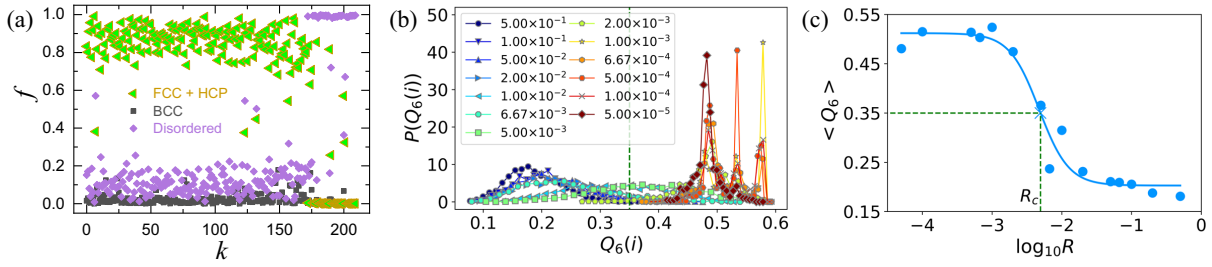

FIG. 2. (a) Fraction f of each system (labeled $k = 1, \ldots, 210$) with a given local structure (fcc, hcp, bcc, or disordered) for a slow cooling rate ($R = 5\times10^{-5}$) in binary LJ systems with $f_B = 0.5$ over the full range of cohesive and interaction energies. (b) Distribution of the local bond orientational order parameter $P[Q_6(i)]$ for systems with $\epsilon_{BB}/\epsilon_{AA} = \epsilon_{AB}/\epsilon_{AA} = 1.0$ over 4 orders of magnitude in cooling rate R. (c) Average bond orientational order $\langle Q_6\rangle$ for the system in (b) versus R. R_c corresponds to the cooling rate at which $\langle Q_6\rangle = (\langle Q_6\rangle_0 + \langle Q_6\rangle_\infty)/2$, which is obtained by fitting the data to a logistic function $(\langle Q_6\rangle - \langle Q_6\rangle_\infty)/(\langle Q_6\rangle_0 - \langle Q_6\rangle_\infty) = \{1 - \tanh[\log_{10}(R/R_c)^{1/\kappa}]\}/2$, where $\langle Q_6\rangle_0$ and $\langle Q_6\rangle_\infty$ are the average bond orientational order in the limits of $R \to 0$ and ∞, and $0 < \kappa < 1$ is the stretching factor. The vertical dashed line in (b) indicates the $\langle Q_6\rangle$ that determines R_c [vertical dashed line in (c)].

$\langle Q_6\rangle = (\langle Q_6\rangle_0 + \langle Q_6\rangle_\infty)/2$, where $\langle Q_6\rangle_0$ and $\langle Q_6\rangle_\infty$ are the values in the limits $R \to 0$ and ∞ limits.

What combination of ϵ_{AA}, ϵ_{BB}, ϵ_{AB}, and f_B controls the GFA in alloys? One possibility is the heat of mixing, which can be generalized for multicomponent alloys as $\Delta H_{\rm mix} = 4\sum_{i\neq j} f_i f_j \Delta H_p(i,j)$ [22]. In Fig. 3(a) we show R_c versus $\Delta H_{\rm mix}$ (normalized by the average cohesive energy $\bar{\epsilon}$) for all binary LJ systems studied. We find little correlation between R_c and $\Delta H_{\rm mix}$ in the simulations [31]. We also assembled a database of 482 metallic glass formers with $n_c = 2, \ldots, 8$ different atomic species, with values of R_c that span 10 orders of magnitude [32]. (See the table provided in the Supplemental Material [32].) The experimental data in Fig. 3(b) is similar to the simulation data; there is no correlation between R_c and $\Delta H_{\rm mix}$, other than $\Delta H_{\rm mix} < 0$ for all metallic glasses. Note that the simulations cover a much wider range of $\Delta H_{\rm mix}/\bar{\epsilon}$ than experiments on metallic glasses, but R_c in the simulations corresponds to only rapid cooling, 10^{13} to 10^9 K/s.

In Figs. 4(a)–4(i) we show contour plots of R_c versus $\bar{\epsilon}_{AB} = 2\epsilon_{AB}/(\epsilon_{AA} + \epsilon_{BB})$ and $\epsilon_- = (\epsilon_{BB} - \epsilon_{AA})/(\epsilon_{AA} + \epsilon_{BB})$ for binary LJ systems with $f_B = 0.1$, 0.2, 0.3, 0.4, 0.5, 0.6, 0.7, 0.8, and 0.9. We find strong correlations between R_c and ϵ_- and $\bar{\epsilon}_{AB}$ for all compositions. However, the contours of equal values of R_c in the ϵ_- and $\bar{\epsilon}_{AB}$ plane are very different for different values of f_B. For example, R_c increases with increasing $\bar{\epsilon}_{AB}$ and increasing ϵ_- for $f_B = 0.1$, whereas R_c increases with increasing $\bar{\epsilon}_{AB}$ and *decreasing* ϵ_- for $f_B \geqslant 0.3$. For $f_B \gg f_A$ with a majority of B atoms and only a small fraction of A atoms, to have good GFA, the cohesive interaction between B atoms must be small compared to that for A atoms with $\epsilon_{BB} - \epsilon_{AA} < 0$ and the interaction between A and B atoms must be strong with $\bar{\epsilon}_{AB} \gg 1$. Similarly, when $f_A \gg f_B$ with a majority of A atoms and only a small fraction of B atoms, to have good GFA, the cohesive interaction between B atoms must be strong (or at least comparable to that between A atoms with $\epsilon_{BB} \approx \epsilon_{AA}$) and the interaction between A and B atoms must be strong with $\bar{\epsilon}_{AB} \gg 1$. Note that the R_c contours are symmetric with respect to switching the labels of atoms A and B, and thus we only show the region $\epsilon_{BB} - \epsilon_{AA} \leqslant 0$.

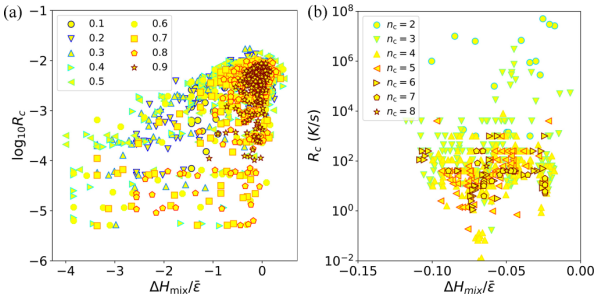

FIG. 3. (a) R_c from simulations of binary LJ systems versus the heat of mixing $\Delta H_{\rm mix}/\bar{\epsilon}$, where $\bar{\epsilon}$ is the average cohesive energy, for nine values of f_B. (b) R_c (in K/s) versus $\Delta H_{\rm mix}/\bar{\epsilon}$ from experiments on 482 metallic glass formers with $n = 2, \ldots, 8$ different atomic species. Note that the scale of R_c in (b) is 10 orders of magnitude, whereas it is 4 orders of magnitude in (a).

In the liquid state, the system is disordered in both the positions and labels of the atoms. The system has only short-range liquidlike positional order and the labels of the same-sized atoms are randomly distributed. As the system is cooled to low temperature, it seeks configurations (both the atomic positions and labels of the atoms) with the lowest potential energy, which will depend on the values of the cohesive energies ϵ_{AA} and ϵ_{BB} and the interaction energy ϵ_{AB}. When $\epsilon_{AA} = \epsilon_{BB}$ and $\epsilon_{AB} = 0$, the fact that there are two species of atoms, A and B, does not affect the ability of the system to find low energy configurations, all labelings of the atoms have the same energy, and thus there is no energetic frustration. When $\epsilon_{AA} \neq \epsilon_{BB}$ and $\epsilon_{AB} > 0$, the random distribution of the atomic labels in the liquid state is no longer the lowest energy configuration. The ability of the system to reach low energy configurations (with order in the atomic labels and positional order) depends on the cooling rate. Thus, the critical cooling rate will depend on ϵ_{AA} and ϵ_{BB}, ϵ_{AB}, and f_B.

We approximate the R_c contours in Fig. 4 as straight lines in the ϵ_- and $\bar{\epsilon}_{AB}$ plane for each f_B and plot the slope k versus f_B in Fig. 5(a). The slope crosses zero near $f_B \approx 0.2$ and reaches a peak value of $k \approx 0.25$ near $f_B \approx 0.8$. As $f_B \to 1$, the system becomes monoatomic with all B atoms, the GFA depends only on ϵ_-, and thus $k \to 0$. As $f_B \to 0$, the

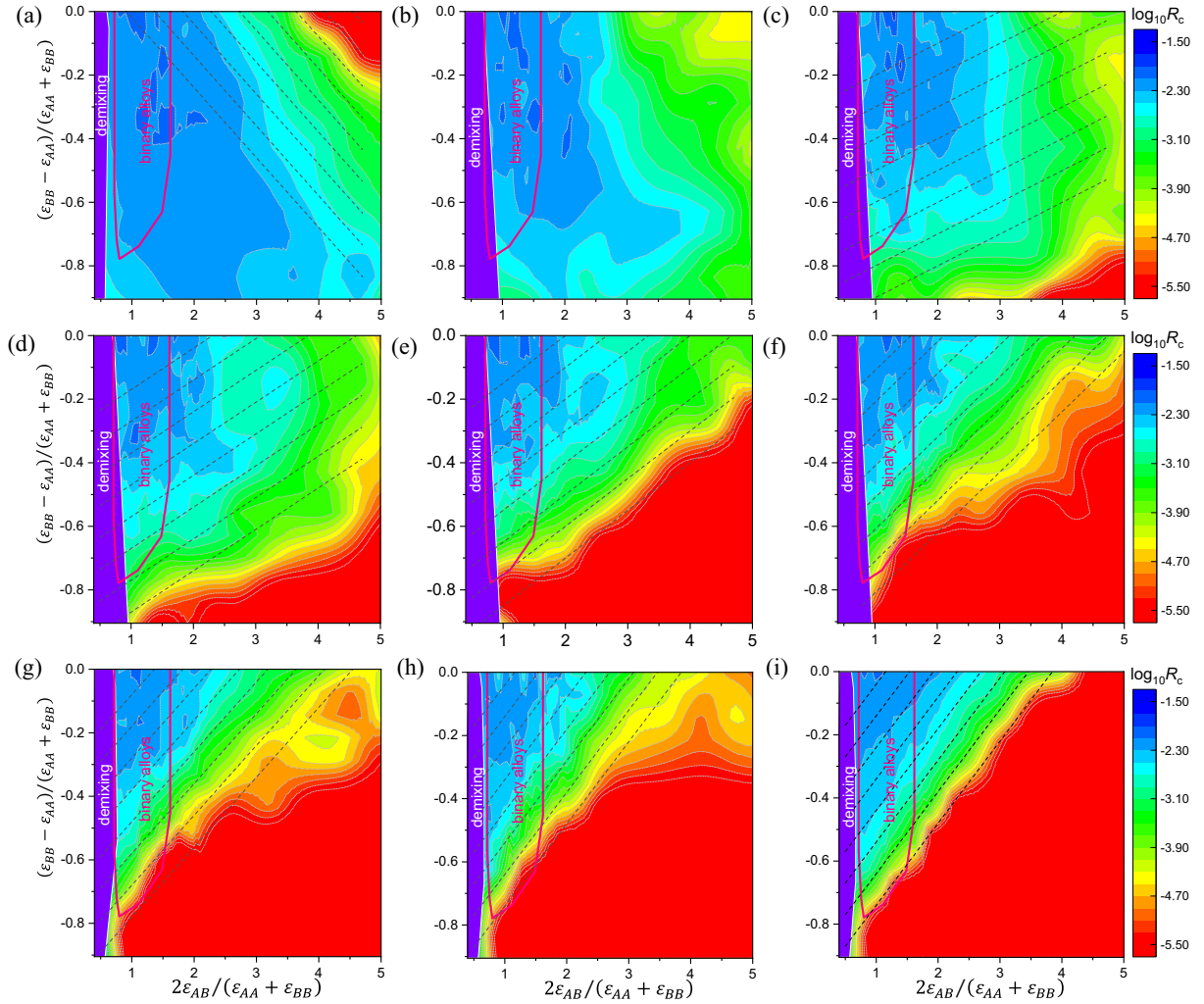

FIG. 4. (a)–(i) Contour plots of equal values of R_c (on a logarithmic scale decreasing from blue to red) versus $\overline{\epsilon}_{AB} = 2\epsilon_{AB}/(\epsilon_{AA}+\epsilon_{BB})$ and $\epsilon_- = (\epsilon_{BB}-\epsilon_{AA})/(\epsilon_{AA}+\epsilon_{BB})$ at $f_B = 0.1, 0.2, 0.3, 0.4, 0.5, 0.6, 0.7, 0.8$, and 0.9. All plots share the same horizontal and vertical axes, as well as the same color scale. Demixing occurs for $\epsilon_{AB} < (\epsilon_{AA}+\epsilon_{BB})/2$ (purple region). The domain of experimentally accessible binary alloys is enclosed within the solid pink curve [cf. Fig. 1(a)]. The dashed lines represent linear approximations of the equal-R_c contours.

system becomes monoatomic with all A atoms, and the GFA is independent of ϵ_- and $\overline{\epsilon}_{AB}$. In this regime, the slope of the contours in the ϵ_- and $\overline{\epsilon}_{AB}$ plane is undefined as indicated by the vertical dashed line in Fig. 5(a). In Fig. 5(b) we show that the data for R_c can be collapsed by plotting $\log_{10} R_c$ versus $[\epsilon_- - k(f_B)\overline{\epsilon}_{AB}]$. We find that the GFA in binary LJ systems obeys a roughly parabolic form:

$$\log_{10} R_c \approx c_1[\epsilon_- - k(f_B)\overline{\epsilon}_{AB}]^2 + \log_{10} R_0, \qquad (4)$$

where $c_1 \approx -2$ gives the concavity and $R_0 \approx 10^{-2}$ is the cooling rate in the $\epsilon_- \to 0$ and $\overline{\epsilon}_{AB} \to 0$ limits.

There are two striking features about the R_c contours in Figs. 4(a)–4(i). First, R_c increases with increasing ϵ_- and $\overline{\epsilon}_{AB}$ for small f_B, indicating that systems with the best GFA possess $\epsilon_{BB} \sim \epsilon_{AA}$ and $\overline{\epsilon}_{AB} \gg 1$. To frustrate crystallization for small f_B, $\epsilon_{BB}/\epsilon_{AA}$ should be as large as possible, approaching $\epsilon_{BB}/\epsilon_{AA} \to 1$. Similarly, large $\overline{\epsilon}_{AB}$ allows the B atoms to act as low mobility defects with root-mean-square (rms) fluctuations $\Delta r_{AB} = \sqrt{\langle r_{AB}^2\rangle - \langle r_{AB}\rangle^2} < \Delta r_{AA}$ in the low-temperature glass, where $\langle r_{AB}\rangle$ is the average separation between an A atom and a Voronoi-neighbor B atom. Additional details of the calculations of Δr_{AB} are included in the Appendix. Second, R_c increases with decreasing ϵ_- and increasing $\overline{\epsilon}_{AB}$ for large f_B. In this case, $\epsilon_{BB} \to 0$ prevents B atoms from clustering. Also, in the large $\overline{\epsilon}_{AB}$ limit, the A atoms act as low mobility defects with rms fluctuations $\Delta r_{AB} < \Delta r_{BB}$ in the low-temperature glass.

In the high-temperature liquid, the identities of the nearest Voronoi neighbors of atoms A and B are completely random.

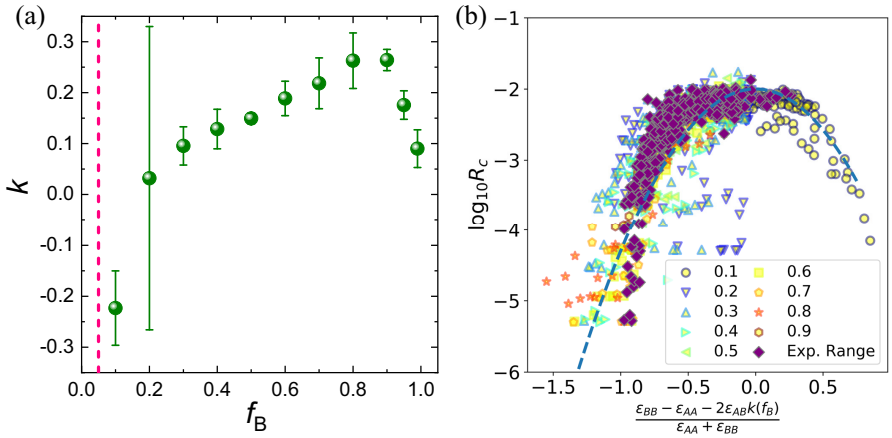

FIG. 5. (a) The best fit slope k of the equal-R_c contour lines in the ϵ_- and $\bar{\epsilon}_{AB}$ plane (in Fig. 4) plotted versus f_B. For $f_B < 0.05$ (vertical dotted line), R_c is uniform and k is undefined. (b) $\log_{10} R_c$ versus $\epsilon_- - k(f_B)\bar{\epsilon}_{AB}$ for all systems studied. The dashed line obeys Eq. (4). Binary LJ systems with ϵ_- and $\bar{\epsilon}_{AB}$ in the experimental range in Fig. 1(a) are indicated by filled diamonds.

As the system cools, the identities of the neighboring atoms for each atom type A and B can deviate from random, and such chemical ordering can affect the GFA. For example, we hypothesize that if the competing crystal has large chemical order, the system will possess large GFA since the A and B species must rearrange significantly to form the crystal. Note that a similar mechanism has been proposed by Song *et al.* [33]. In this work they show that local atomic ordering in the crystal phase of $Cu_{50}Zr_{50}$ results in a much lower atom attachment rate to the crystal nucleus during crystallization, which gives rise to enhanced GFA. To assess the hypothesis of a connection between local order and high GFA, we measured the chemical ordering [i.e., the probability $p_A(N_B)$ for an A atom to have N_B B nearest neighbors when $f_A > f_B$ or the

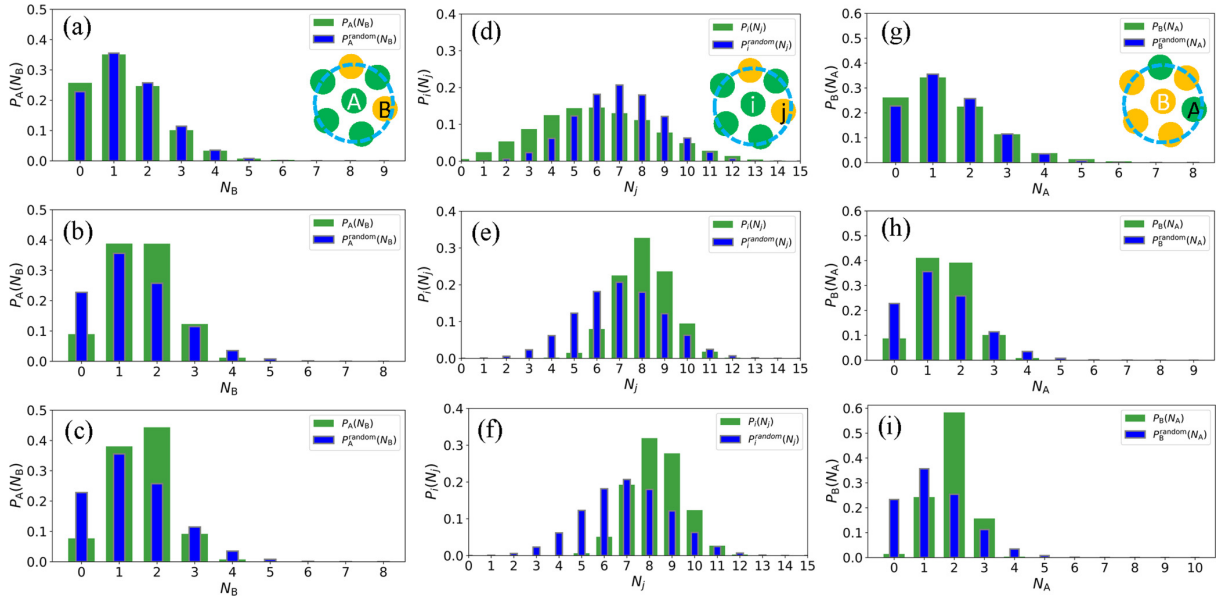

FIG. 6. The probability $P_i(N_j)$ with $i \neq j$ for an i atom to have N_j Voronoi nearest neighbors for (a)–(c) $f_B = 0.1$, (d)–(f) 0.5, and (g)–(i) 0.9 in binary LJ systems cooled at $R = 5\times10^{-5}$ (green wide bars), which yields systems with local fcc order, for combinations of ϵ_- and $\bar{\epsilon}_{AB}$ with increasing GFA. We also show $P_i^{\text{random}}(N_j)$ (thin blue bars) for systems with the same structure, but randomized atom types for the nearest neighbors. For $f_B = 0.1$, we only consider $P_A(N_B)$ since A is the majority species. For $f_B = 0.9$, we only consider $P_B(N_A)$ since B is the majority species. The specific parameters for each panel are as follows: (a) $R_c = 7.4\times10^{-3}$, $\bar{\epsilon}_{AB} = 0.83$, $\epsilon_- = -0.67$, (b) $R_c = 7.5\times10^{-4}$, $\bar{\epsilon}_{AB} = 5.0$, $\epsilon_- = -0.67$, (c) $R_c = 2.5\times10^{-4}$, $\bar{\epsilon}_{AB} = 4.17$, $\epsilon_- = -0.11$, (d) $R_c = 3.3\times10^{-4}$, $\bar{\epsilon}_{AB} = 0.83$, $\epsilon_- = -0.67$, (e) $R_c = 2.8\times10^{-4}$, $\bar{\epsilon}_{AB} = 4.17$, $\epsilon_- = -0.11$, (f) $R_c \leqslant 10^{-6}$, $\bar{\epsilon}_{AB} = 5.0$, $\epsilon_- = -0.67$, (g) $R_c = 6.6\times10^{-4}$, $\bar{\epsilon}_{AB} = 0.83$, $\epsilon_- = -0.67$, (h) $R_c = 5.6\times10^{-5}$, $\bar{\epsilon}_{AB} = 4.17$, $\epsilon_- = -0.11$, and (i) $R_c \leqslant 10^{-6}$, $\bar{\epsilon}_{AB} = 5.0$, $\epsilon_- = -0.67$.

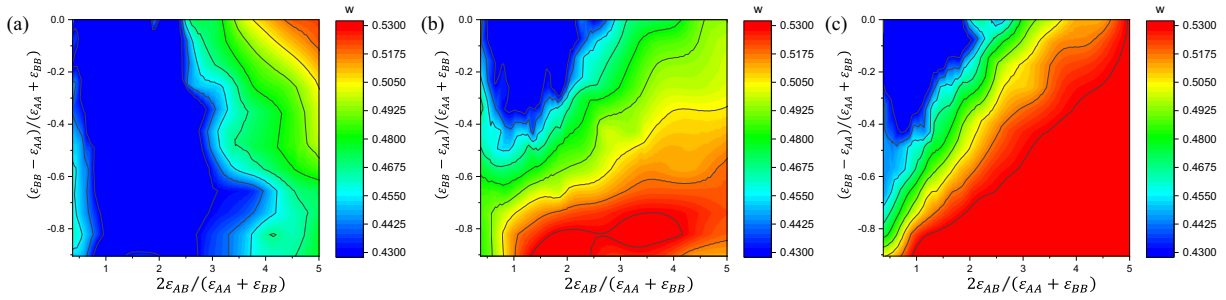

FIG. 7. Contour plots of the local fivefold symmetric order parameter W as a function of ϵ_- and $\overline{\epsilon}_{AB}$ for low-temperature glasses generated using $R = 10^{-2}$ for (a) $f_B = 0.1$, (b) 0.5, and (c) 0.9. W increases from blue to red. The contours for W in (a)–(c) are similar to the contours for R_c presented in Figs. 4(a), 4(e) and 4(i).

probability $p_B(N_A)$ for a B atom to have N_A A nearest neighbors when $f_B > f_A$] at a slow cooling rate with significant fcc order. In Fig. 6 we show $p_i(N_j)$ (with $i \neq j$) for systems with $f_B = 0.1, 0.5, 0.9$ in Figs. 6(a)–6(f), and 6(g)–6(i), respectively. R_c decreases from Figs. 6(a) to 6(c), from Figs. 6(d) to 6(f), and from Figs. 6(g) to 6(i). In each panel we compare $p_i(N_j)$ to $p_i^{\text{random}}(N_j)$, where we keep the low-temperature structure of the system and randomly assign the labels of the nearest neighbors. We find that the GFA increases with the chemical order, $\sum_{N_j} |p_i(N_j) - p_i^{\text{random}}(N_j)|$, of the competing crystal.

To further understand how energetic frustration influences the GFA of binary alloys in the absence of geometric frustration, we performed local structural analysis using Voronoi tessellation [34]. Using this analysis, we can calculate the Voronoi index $\langle n_3, n_4, n_5, n_6\rangle$, which is a list of integers that gives the number of faces with three, four, five, and six edges. For example, the Voronoi index for an icosahedron is $\langle 0, 0, 12, 0\rangle$. Although $\langle 0, 0, 12, 0\rangle$ is the dominant local structural motif in CuZr-based metallic glasses, it is not the dominant motif in many other glass-forming alloys, such as Mg-Cu-Y, Ni-P, Pd-Si, and Ni-Zr. However, local fivefold symmetry is significant in these systems. We can define the average degree of fivefold local structural order: $W = \langle n_5/\sum_{i=3}^{6} n_i\rangle$ [16]. Since local fivefold order is incompatible with global fcc and related crystalline order, W quantifies the degree of frustration to crystallization. In Fig. 7 we show that large fivefold order is also observed in systems with only energetic frustration, and no geometric frustration. Furthermore, we show that there is a strong correlation between large fivefold order W and small values of the critical cooling rate R_c (i.e., good GFA). Thus, both geometric frustration and energetic frustration (e.g., cohesive energy differences) can lead to pronounced fivefold order that lowers the nucleation rate due to an increase in the interfacial energy between the liquid and crystal phases.

IV. CONCLUSIONS

By decoupling geometric and energetic frustration, we have shown that the GFA is not strongly correlated to the heat of mixing, which involves the particular combination of variables $(\epsilon_{BB} + \epsilon_{AA})/2\epsilon_{AA} - \epsilon_{AB}/\epsilon_{AA}$. Instead, we find that the GFA is strongly correlated with ϵ_- (i.e., the difference in the cohesive energies, not the sum) and $\overline{\epsilon}_{AB}$, and we identified the f_B-dependent combination of ϵ_- and $\overline{\epsilon}_{AB}$ that controls the GFA for binary LJ systems. We emphasize that it was important to study regions of the ϵ_- and $\overline{\epsilon}_{AB}$ parameter space that were beyond the experimental range of metallic glasses to fully understand the parameter dependence of the GFA. This work will motivate several important future studies. First, we encourage researchers to experimentally characterize the GFA of binary alloys containing elements with nearly the same metallic radii, yet with large energetic frustration. Second, we are now in a position to understand theoretically the GFA of binary LJ systems with both geometric and energetic frustration. By tuning both the atomic size ratio and cohesive energy difference, we will study how energetic frustration couples to geometric frustration to determine the GFA of binary alloys. From our preliminary studies, we find that the atomic species with the larger metallic radius possesses the larger cohesive energy for binary alloys with the best GFA. These results are consistent with several metal-metal binary metallic glass formers found in experiments, such as Cu-Zr, Ni-P, and Ni-Nb. A more complete study of binary alloys with both energetic and geometric frustration is currently being performed.

ACKNOWLEDGMENTS

The authors acknowledge support from NSF MRSEC Grant No. DMR-1119826 (Y.-C.H.) and NSF Grants No. CMMI-1462439 (C.O.) and No. CMMI-1463455 (M.S.). This work was supported by the High Performance Computing facilities operated by, and the staff of, the Yale Center for Research Computing.

APPENDIX

In this Appendix we include five brief sections that provide additional details about the results presented in the main text. The five sections are as follows: (1) Finite-size effects of the critical cooling rate, (2) identification of the parameter space where cavitation occurs, (3) comparisons of the critical cooling rate when cooling at different fixed pressures, (4) common neighbor analysis of structural order over a wide

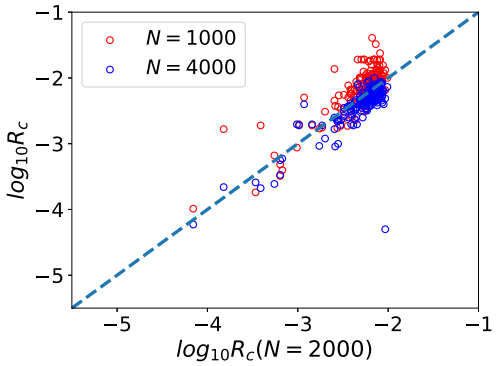

FIG. 8. Comparison of the critical cooling rate R_c obtained at $N = 2000$ to R_c at $N = 1000$ (open red circles) and 4000 (open blue circles) for $f_B = 0.1$. The dashed line with slope one and zero vertical intercept indicates when the critical cooling rates at different system sizes are the same.

range of cooling rates, and (5) root-mean-square position fluctuations among nearest neighbor atoms.

1. Finite-size effects of the critical cooling rate

We carried out studies of the glass-forming ability of binary LJ alloys, by measuring the critical cooling rate, over the full range of ϵ_- and $\overline{\epsilon}_{AB}$ for $N = 1000$, 2000, and 4000 to understand the system-size effects of R_c. We show in Fig. 8 that the system-size dependence of R_c is weak, and thus we show results for $N = 2000$ in the main text.

2. Identification of the parameter space where cavitation occurs

During the cooling process to create low-temperature glasses, cavities can form when the number density ρ or pressure P of the system is too low. To ensure that all systems are homogeneous, we checked for cavity formation in the low-temperature glass states. To determine whether a cavity formed, we divided the cubic volume into 125 equal-sized boxes and determined the fraction of boxes $f_{\rm void}$ that did not possess any atoms. For systems with $N = 2000$ atoms, each box will contain on average 16 atoms if they are distributed homogeneously. As shown in Fig. 9, LJ systems can cavitate when they are cooled at constant volume (with $\rho = 1.0$), while cavity formation is rare when they are cooled at constant pressure $P_0 = 10$. Thus, most of our studies were performed at constant pressure with $P_0 = 10$. In addition, we have found that the critical cooling rates R_c for systems that do not cavitate are similar when cooled at constant volume (at $\rho = 1.0$) and constant pressure $P_0 = 10$.

3. Comparisons of the critical cooling rate when cooling at different fixed pressures

Most of the studies of the critical cooling rate R_c for binary LJ systems were performed at constant pressure. In Fig. 10 we show results for R_c over the full range of ϵ_- and $\overline{\epsilon}_{AB}$ generated by cooling at constant pressure with $P_0 = 0.1$ and 10. For most of the data, the critical cooling rates are similar for the two pressures. However, there is some dependence of R_c on

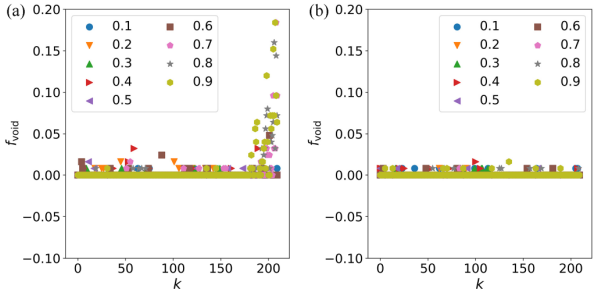

FIG. 9. The fraction $f_{\rm void}$ of each low-temperature glass (labeled $k = 1, 2, \ldots, 210$) that possesses voids when cooled using $R = 5\times10^{-5}$ at (a) constant volume (with reduced number density $\rho = 1.0$) and at (b) constant pressure with $P_0 = 10$. We show systems in which the fraction of B atoms is varied from $f_B = 0.1$ to 0.9.

the pressure for the systems with low values of R_c, e.g., the minimum R_c is $\approx10^{-5.5}$ for $P_0 = 10$, while it is $\approx10^{-4.5}$ for $P_0 = 0.1$.

4. Common neighbor analysis of structural order over a wide range of cooling rates

To study the crystallization process of binary LJ alloys, we analyzed the structural order as a function of the cooling rate using adaptive common neighbor analysis [30]. As shown in Fig. 11(a) for $f_B = 0.5$, at high cooling rates, all atoms exist in disordered local environments. As the cooling rate decreases, local crystalline order (fcc, hcp, and bcc) begins to appear as shown in Figs. 11(b) and 11(c). However, at the lowest cooling rates, the systems form crystals with only fcc and hcp order, with no bcc order. We find similar results for the other values of f_B studied. These results suggest that the lowest energy

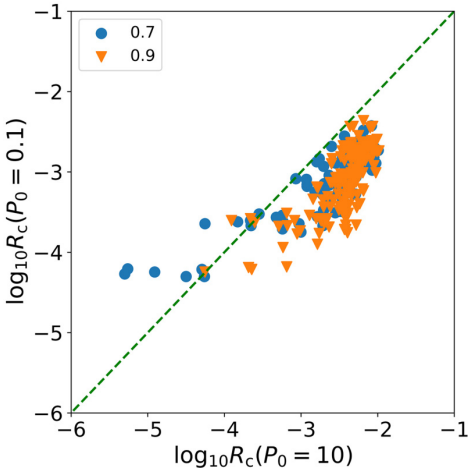

FIG. 10. Critical cooling rate R_c of binary LJ systems at two compositions, $f_B = 0.7$ (filled circles) and 0.9 (downward triangles), and many values of $\overline{\epsilon}_{AB} = 2\epsilon_{AB}/(\epsilon_{AA} + \epsilon_{BB})$ and $\epsilon_- = (\epsilon_{BB} - \epsilon_{AA})/(\epsilon_{AA} + \epsilon_{BB})$ when cooling at constant pressure $P_0 = 0.1$ (vertical axis) and 10 (horizontal axis). The dashed line has slope one and zero vertical intercept.

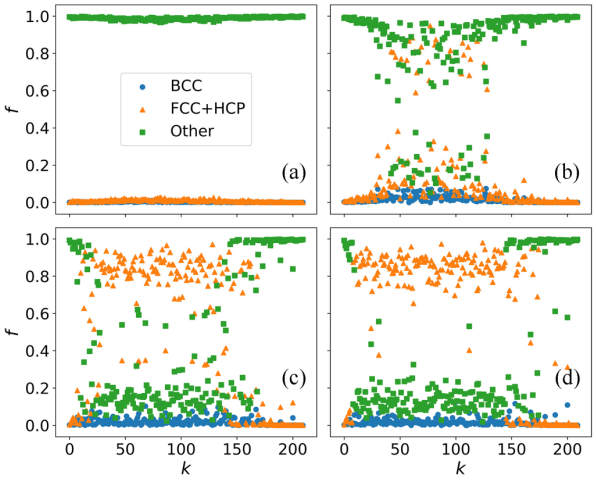

FIG. 11. Fraction f of each system (labeled $k = 1, 2, \ldots, 210$) with a given local structure, fcc and hcp (triangles), bcc (circles), or disordered (squares), at four cooling rates, (a) $R = 5\times10^{-2}$, (b) 5×10^{-3}, (c) 10^{-3}, and (d) 5×10^{-4} in binary LJ systems with $f_B = 0.5$ over the full range of cohesive energies and interaction energies between A and B atoms.

state of binary LJ alloys over the full range of ϵ_-, $\bar{\epsilon}_{AB}$, and f_B is the close packed hcp and fcc crystals.

In the probability distributions of the bond-orientational order parameter $P[Q_6(i)]$ in Fig. 2(b), we find a peak near $Q_6(i) \approx 0.535$ between peaks at $Q_6(i) \approx 0.485$ (corresponding to hcp order) and $\approx$0.575 (corresponding to fcc order) even for systems generated using low cooling rates. The value $Q_6(i) \approx 0.535$ is close to the value of $Q_6(i) = 0.511$ for

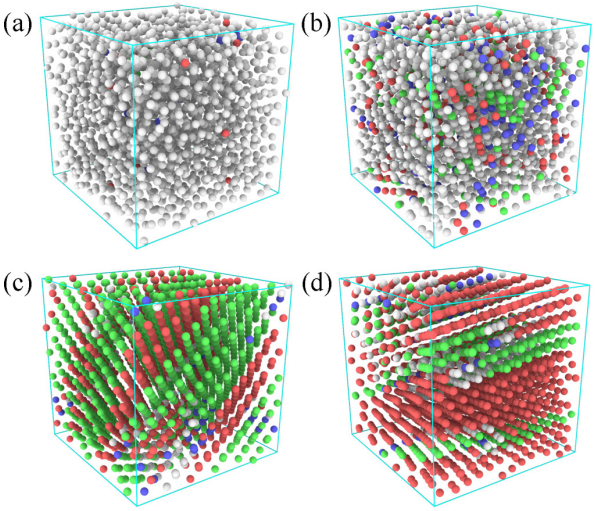

FIG. 12. Snapshots of the low-temperature glasses of binary LJ systems with $\epsilon_{BB}/\epsilon_{AA} = \epsilon_{AB}/\epsilon_{AA} = 1.0$ and $f_B = 0.5$ at cooling rates (a) $R = 5\times10^{-2}$, (b) 5×10^{-3}, (c) 5×10^{-4}, and (d) 5×10^{-5}, where $R_c \approx 5\times10^{-3}$. Atoms are colored according to the structure of their local environment, i.e., green: fcc, red: hcp, blue: bcc, and white: disordered.

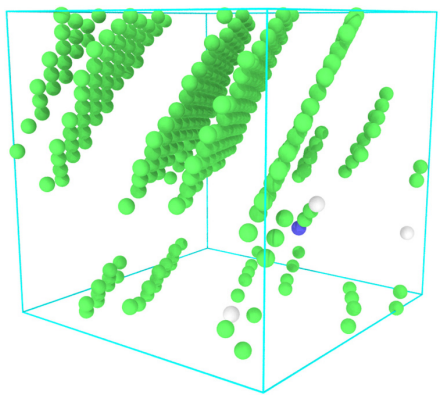

FIG. 13. The same snapshot as in Fig. 12(c), but now only showing atoms with $0.53 < Q_6(i) < 0.54$. We find that the atoms with $Q_6(i)$ in this narrow range are adjacent to regions with local hcp order. Note that the atoms are colored in the same way as Fig. 12.

bcc order. To investigate this intermediate peak, we visualize atoms with $0.53 < Q_6(i) < 0.54$ in Fig. 13. These atoms possess local fcc order, not bcc order, but are located at the interface with local hcp order, which lowers their values of $Q_6(i)$.

5. Root-mean-square position fluctuations among nearest neighbor atoms

The root-mean-square position fluctuations $\Delta r_{ij} = \sqrt{\langle r_{ij}^2\rangle - \langle r_{ij}\rangle^2}$ are calculated using the low temperature solids at a low cooling rate $R = 5\times10^{-5}$ at constant pressure with $P_0 = 10$. For $f_B = 0.1$ we consider the A atoms and calculate the separations between their Voronoi neighbors, r_{AA} for A neighbors and r_{AB} for B neighbors. Similarly for $f_B = 0.9$, we consider the B atoms and calculate the separations between their Voronoi neighbors, r_{AB} for A neighbors and

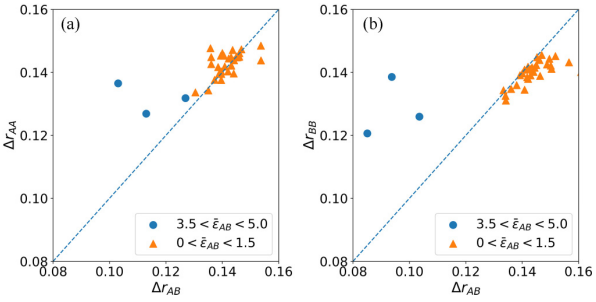

FIG. 14. The root-mean-square separation fluctuations, (a) Δr_{AA} versus Δr_{AB} and (b) Δr_{BB} versus Δr_{AB}, where $\Delta r_{ij} = \sqrt{\langle r_{ij}^2\rangle - \langle r_{ij}\rangle^2}$, for binary LJ systems with (a) $f_B = 0.1$ and (b) 0.9 for the low-temperature solids obtained using a low cooling rate $R = 5\times10^{-5}$ (at constant pressure with $P_0 = 10$). The filled circles and triangles indicate large and small values of $\bar{\epsilon}_{AB}$, respectively. $\Delta r_{AA} > \Delta r_{AB}$ for $f_B = 0.1$ and $\Delta r_{BB} > \Delta r_{AB}$ for $f_B = 0.9$. For both (a) and (b), the variable ϵ_- occurs in the narrow range, $-0.2 < \epsilon_- < 0$. Similar results were also obtained at other values of f_B.

r_{BB} for B neighbors. For large $\bar{\epsilon}_{AB}$, the separation between different species is smaller than that between similar species, which makes the minor species act as low mobility defects. (See Fig. 14.) The minor species will then hinder crystallization of the major species, and yield a smaller critical cooling rate.

[1] J. Schroers, Bulk metallic glasses, Phys. Today **66**(2), 32 (2013).

[2] M. D. Demetriou, M. E. Launey, G. Garrett, J. P. Schramm, D. C. Hofmann, W. L. Johnson, and R. O. Ritchie, A damage-tolerant glass, Nat. Mater. **10**, 123 (2011).

[3] W. H. Wang, The elastic properties, elastic models and elastic perspectives of metallic glasses, Prog. Mater. Sci. **57**, 487 (2012).

[4] B. Zberg, P. J. Uggowitzer, and J. F. Löffler, MgZnCa glasses without clinically observable hydrogen evolution for biodegradable implants, Nat. Mater. **8**, 887 (2009).

[5] Z. Lu and C. Liu, A new glass-forming ability criterion for bulk metallic glasses, Acta Mater. **50**, 3501 (2002).

[6] A. Inoue, Stabilization of metallic supercooled liquid and bulk amorphous alloys, Acta Mater. **48**, 279 (2000).

[7] D. Xu, B. Lohwongwatana, G. Duan, W. L. Johnson, and C. Garland, Bulk metallic glass formation in binary Cu-rich alloy series—$Cu_{100-x}Zr_x$ ($x = 34$, 36, 38.2, 40 at.%) and mechanical properties of bulk $Cu_{64}Zr_{36}$ glass, Acta Mater. **52**, 2621 (2004).

[8] Y. Li, Q. Guo, J. A. Kalb, and C. V. Thompson, Matching glass-forming ability with the density of the amorphous phase, Science **322**, 1816 (2008).

[9] M. B. Tang, D. Q. Zhao, M. X. Pan, and W. H. Wang, Binary Cu-Zr bulk metallic glasses, Chin. Phys. Lett. **21**, 901 (2004).

[10] A.-P. Tsai, A. Inoue, and T. Masumoto, Ductile Al-Cu-V amorphous alloys without metalloid, Metal. Trans. A **19**, 391 (1988).

[11] L. Zhong, J. Wang, H. Sheng, Z. Zhang, and S. X. Mao, Formation of monatomic metallic glasses through ultrafast liquid quenching, Nature (London) **512**, 177 (2014).

[12] K. Zhang, M. Wang, S. Papanikolaou, Y. Liu, J. Schroers, M. D. Shattuck, and C. S. O'Hern, Computational studies of the glass-forming ability of model bulk metallic glasses, J. Chem. Phys. **139**, 124503 (2013).

[13] H. Shintani and H. Tanaka, Frustration on the way to crystallization in glass, Nat. Phys. **2**, 200 (2006).

[14] D. B. Miracle, A structural model for metallic glasses, Nat. Mater. **3**, 697 (2004).

[15] H. W. Sheng, W. K. Luo, F. M. Alamgir, J. M. Bai, and E. Ma, Atomic packing and short-to-medium-range order in metallic glasses, Nature (London) **439**, 419 (2006).

[16] Y. C. Hu, F. X. Li, M. Z. Li, H. Y. Bai, and W. H. Wang, Five-fold symmetry as indicator of dynamic arrest in metallic glass-forming liquids, Nat. Commun. **6**, 8310 (2015).

[17] Y. Q. Cheng, E. Ma, and H. W. Sheng, Atomic Level Structure in Multicomponent Bulk Metallic Glass, Phys. Rev. Lett. **102**, 245501 (2009).

[18] G. Cargill and F. Spaepen, Description of chemical ordering in amorphous alloys, J. Non-Cryst. Solids **43**, 91 (1981).

[19] S. Nosé, A unified formulation of the constant temperature molecular dynamics methods, J. Chem. Phys. **81**, 511 (1984).

[20] W. G. Hoover, Canonical dynamics: Equilibrium phase-space distributions, Phys. Rev. A **31**, 1695 (1985).

[21] G. J. Martyna, D. J. Tobias, and M. L. Klein, Constant pressure molecular dynamics algorithms, J. Chem. Phys. **101**, 4177 (1994).

[22] A. Takeuchi and A. Inoue, Calculations of mixing enthalpy and mismatch entropy for ternary amorphous alloys, Mater. Trans. **41**, 1372 (2000).

[23] A. M. Halpern, From dimer to crystal: Calculating the cohesive energy of rare gas solids, J. Chem. Ed. **89**, 592 (2012).

[24] A. Takeuchi and A. Inoue, Classification of bulk metallic glasses by atomic size difference, heat of mixing and period of constituent elements and its application to characterization of the main alloying element, Mater. Trans. **46**, 2817 (2005).

[25] T. Köddermann, D. Paschek, and R. Ludwig, Molecular dynamic simulations of ionic liquids: A reliable description of structure, thermodynamics and dynamics, Chem. Phys. Chem. **8**, 2464 (2007).

[26] J. de Andrade, E. S. Böes, and H. Stassen, Computational study of room temperature molten salts composed by 1-alkyl-3-methylimidazolium cations-force-field proposal and validation, J. Phys. Chem. B **106**, 13344 (2002).

[27] F. London, The general theory of molecular forces, Trans. Faraday Soc. **33**, 8 (1937).

[28] P. J. Steinhardt, D. R. Nelson, and M. Ronchetti, Bond-orientational order in liquids and glasses, Phys. Rev. B **28**, 784 (1983).

[29] W. Mickel, S. C. Kapfer, G. E. Schröder-Turk, and K. Mecke, Shortcomings of the bond orientational order parameters for the analysis of disordered particulate matter, J. Chem. Phys. **138**, 044501 (2013).

[30] A. Stukowski, Structure identification methods for atomistic simulations of crystalline materials, Model. Simul. Mater. Sci. Eng. **20**, 045021 (2012).

[31] Y. Li, S. Zhao, Y. Liu, P. Gong, and J. Schroers, How many bulk metallic glasses are there? ACS Comb. Sci. **19**, 687 (2017).

[32] See Supplemental Material at http://link.aps.org/supplemental/10.1103/PhysRevMaterials.3.085602 for the database of the critical cooling rates of various MGs from experiments.

[33] H. Song, Y. Sun, F. Zhang, C. Z. Wang, K. M. Ho, and M. I. Mendelev, Nucleation of stoichiometric compounds from liquid: Role of the kinetic factor, Phys. Rev. Mater. **2**, 023401 (2018).

[34] C. H. Rycroft, G. S. Grest, J. W. Landry, and M. Z. Bazant, Analysis of granular flow in a pebble-bed nuclear reactor, Phys. Rev. E **74**, 021306 (2006).